Research Article

Na Yang, Chiemi Oka, Seiichi Hata and Junpei Sakurai*

# Fabrication of textured substrates for dye-sensitized solar cells using polydimethylsiloxane nanoimprint lithography

https://doi.org/10.1515/aot-2019-0010
Received January 16, 2019; accepted June 4, 2019; previously published online June 29, 2019

**Abstract:** We proposed a fabrication of nanoimprinted textures on a front glass/transparent conductive oxide interface for dye-sensitized solar cells (DSSCs). These textures were fabricated through polydimethylsiloxane (PDMS) nanoimprint lithography on organosilsesquioxane solution. The texture structures were estimated via optical simulation. Master molds were anodic aluminum oxide templates with nano-texture (N-Tx) and micro-nano double texture (D-Tx). Meanwhile, replicate molds used a hard PDMS. Fluorine-doped tin oxide and titanium dioxide were deposited on textured glass substrates to generate electrodes for DSSCs. Unlike the DSSCs without texture, textured DSSCs realized 11.4% (N-Tx) and 10% (D-Tx) improvement in conversion efficiency.

**Keywords:** dye-sensitized solar cells; inner AR; polydimethylsiloxane nanoimprint lithography; textures.

## 1 Introduction

Light management, which improves module power by increasing light absorption in active layers, is a key technique for solar modules. Antireflection (AR) coatings or textures on a sunny-side glass are most effective technologies and used worldwide in all photovoltaic modules/cells [1–4] because incident light loses largely at the interface between air (refractive index of 1.00) and front glass (refractive index of 1.52 [5]). However, the effects of AR coating or texture degrade easily due to outside weather and organic contamination. Meanwhile, enhancing the light path within the absorption layers by light trapping textures inside the front glass is vital in thin-film solar modules [1, 2, 6–9].

The surface texturing for light trapping has two roles: 'inner AR' and 'light scattering'. Generally, thin-film solar cells use transparent conductive oxides (TCO) as the front electrode. Commercial thin-film solar modules also adopted natural-textured TCOs, such as fluorine-doped $SnO_2$ (FTO) deposited through low-pressure chemical vapor deposition (LPCVD) [10] or spray pyrolysis deposition (SPD) [11] and aluminum-doped zinc oxide (AZO) deposited through LPCVD [1, 2, 8, 10]. These TCOs are deposited on a flat glass. The refractive index of TCO is approximately 2.00 at 632 nm [12]; thus, a few percent reflections on glass and TCO occur.

To reduce light loss, inserting silicon nitride, which has a refractive index, in between the glass and AZO as inner AR coatings at the glass/AZO interface reduces the reflection to 1.6% [13]. Hence, this inner AR will not be degraded. Moreover, submicron structure layers on the glass/TCO interface were fabricated via UV nanoimprint lithography (NIL) as the inner AR structure, including light trapping effect [8, 9]. These textures improved the efficiency of thin-film solar cells. However, these structures may degrade due to the reliability and weatherability of NIL resins, for example, yellowing. In addition, these inner AR structures induced the degradation of the light absorption layer in thin-film amorphous silicon or tandem devices [8].

Dye-sensitized solar cells (DSSCs) attracted a remarkable interest because of their low material cost, simple construction, and color potential, transparency, and flexibility. However, with a cell efficiency of approximately 11.9%, which is less than half of a crystalline silicon solar cell [14], additional improvement in DSSCs is required. Figure 1A shows the construction of a conventional DSSC

***Corresponding author: Junpei Sakurai,** Nagoya University, Graduate Department of Micro-Nano Mechanical Science and Engineering, Nagoya, Japan, e-mail: junpei.sakurai@mae.nagoya-u.ac.jp
**Na Yang:** Nagoya University, Graduate School of Engineering, Nagoya, Japan
**Chiemi Oka and Seiichi Hata:** Nagoya University, Graduate Department of Micro-Nano Mechanical Science and Engineering, Nagoya, Japan

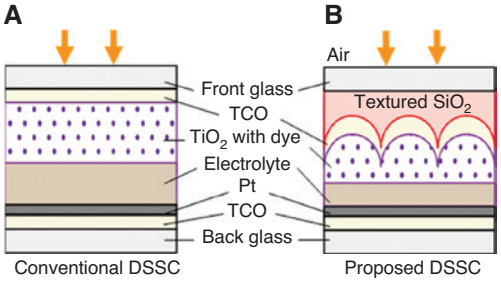


**Figure 1:** Schematic illustrations of DSSCs.
(A) Conventional DSSC. (B) Proposed DSSC.

(Figure 1). As observed in the figure, a DSSC comprises a front glass coated with FTO (FTO glass), nanoparticle $TiO_2$ layer, electrolytes, and back-side glass coated platinum. The $TiO_2$ layer adsorbed with a photosensitive dye acts as an anode and generates electrons when light passes through. Hence, apart from the dye performance improvement, increasing incident light into the $TiO_2$ layer and light trapping in $TiO_2$ are important in the enhancement of DSSC efficiency.

Two types of light trapping on the front glass in DSSCs were reported. One is the FTO layer with textured structures. They used FTO glasses with various morphology of FTO under various SPD conditions [11] and with a textured structure etched by RIE [15]. Another is the $TiO_2$ layer with a textured structure, fabricated by imprinting [16, 17], patterned screen printing [18], and anodic titanium oxide [19]. Mainly researches used commercial FTO glasses. Meanwhile, textured back substrates that have a two-dimensional periodic structure for increasing the reflection applied to DSSCs were reported [20]. These textured structures were fabricated on an Si substrate using solvent suspension/inorganic nanoparticle pastes, such as ZnO, ITO, $TiO_2$, and $SiO_2$, by stamping polydimethylsiloxane (PDMS) molds. These DSSCs improved power conversion efficiency by light trapping.

Figure 1B shows our proposed DSSC using a textured front glass through PDMS NIL on organosilsesquioxane (OSQ) solution similar to hydrogen SQ [21]. The textured substrate at the glass/TCO interface was reported to apply for thin-film Si solar cells [1, 2, 8, 9] because TCO was coated by the LP-CVD process in the commercial production of the thin-film Si solar modules. These textured glasses and FTO are also expected to improve DSSC efficiency in three effects: (1) less light loss (reflection) at the glass/FTO interface, (2) longer light path owing to the scattering into the $TiO_2$ layer, and (3) reduction of electrical resistance associated with the increase in the FTO/$TiO_2$ surface area. In this research, we adopted the FTO fabricated by SPD to low-cost fabrication. Thus, we utilized OSQ for textured material regardless of its low refractive index (n = 1.41). Although excellently textured materials have refractive index in between the glass and FTO, this disadvantage can be compensated through a designed texture structure. Meanwhile, textured materials must show high heat resistance because the FTO coating is performed at 450°C in air. After baking, the used OSQ changed and possessed a characteristic similar to $SiO_2$, which had high heat resistance. Here, baked OSQ is expressed as $SiO_2$.

First, we calculated and designed two textures through optical simulation. Two master templates, with nano and micro-nano double concave structures, were fabricated via anodic oxidation of aluminum and wet etching. Then, PDMS molds were replicated, from which textures were transferred onto the glass substrate through PDMS NIL. The assumed effects (1) and (2) were confirmed by measuring the reflectance and diffuse transmittance of textured glass substrates, whereas effect (3) was examined by observing the surface topography of the substrates after $TiO_2$ deposition. Finally, the properties of DSSCs were evaluated under AM 1.5 illumination.

## 2 Experimental

### 2.1 Optical simulation

Textured structures with high aspect ratio show excellent AR effect over a broad wavelength range [22]. However, the designs of textured structures were restricted to a concave structure, considering the characteristics of the used OSQ and fabrication processing of DSSC. This is because a high aspect ratio structure had some problems, such as large shrink of OSQ and low coverage of FTO or $TiO_2$ on these structures. Moreover, the texture height is less than 1 μm because when the thickness of OSQ exceeds 1 μm, the baked OSQ film tends to break by stressing themselves. To optimize the scale of the texture structure, the reflectance (from the air to the $TiO_2$ layer) of the concave structure with a range of pitches (from 100 nm to 1000 nm) and depths (half of the pitch) were calculated using Gsolver (Grating Solver Development Co., Saratoga Springs, UT, USA).

Figure 2 shows the schematic of the simulation model. As observed in the figure, light in the air passes through the glass, textured $SiO_2$, and FTO and finally arrives at the $TiO_2$ layer. Table 1 presents the refractive index and thickness of each layer (Table 1). As a standard sample, the reflectance of a conventional non-textured model with air/glass/flat FTO/$TiO_2$ layers was also simulated, as shown in the table. Table 2 summarizes the average reflectance in the wavelength ranging from 400 nm to 800 nm (Table 2). In addition, the texture with a pitch of 400 nm and a depth of 200 nm demonstrates the lowest reflectance. However, our attempt to fabricate a periodic structure through photolithography or direct laser writing was restricted using our experimental equipment. Further, considering that a random surface texture causes scattering [23], we believed

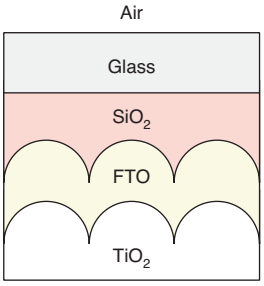


**Figure 2:** Schematic image of simulation model.

**Table 1:** Parameters of simulation model.

| Layer | Air | Glass | $SiO_2$ | FTO | $TiO_2$ |
|---|---|---|---|---|---|
| Refractive index | 1.00 | 1.51 | 1.41 | 2.01 | 2.60 |
| Thickness (μm) | | 700 | 1 | 0.8 | |

**Table 2:** Average reflectance in the wavelength range from 400 to 800 nm of simulation.

| Pitch (nm) | Flat | 100 | 200 | 400 | 600 | 800 | 1000 |
|---|---|---|---|---|---|---|---|
| Depth (nm) | | 50 | 100 | 200 | 300 | 400 | 500 |
| Reflectance (%) | 6.5 | 9.0 | 4.4 | 2.5 | 9.3 | 4.2 | 6.5 |

that fabricating random texture on the scale of 400 nm is feasible. Anodic oxidation is a convenient method to realize a porous structure with a pitch of approximately 400 nm [24–26]. Moreover, by adjusting anodization and wet etching conditions, a random texture with a micro-nano double structure was realized.

## 2.2 Fabrication of textured glass substrates

Figure 3 illustrates the fabrication process of the textured substrates (Figure 3). As shown in the figure, the master molds are anodic aluminum oxide (AAO) templates with modifications in conditions for different textures. Replicate molds utilized a hard PDMS. The textures were transferred on glass substrates through PDMS NIL using OSQ solution.

## 2.3 Master molds

Figure 3A shows the fabrication process of two types of master mold. First, porous aluminum oxide ($Al_2O_3$) grew on a pretreated aluminum (Al) sheet as a result of anodization (Figure 3A-1, 2). Second, the pore diameter of $Al_2O_3$ was widened, and the thickness was reduced through wet etching (Figure 3A-3). Third, the nano-texture (N-Tx) was obtained (Figure 3A-3). With further etching, porous $Al_2O_3$ formed when the first AAO was removed completely. Fourth, the concave texture of micrometer scale appeared on the Al substrate (Figure 3A-4). This substrate was treated through the second anodization (Figure 3A-5). Finally, porous $Al_2O_3$ formed by the second AAO was also second etched, and then double texture (D-Tx) was obtained (Figure 3A-6).

Pretreatments primarily followed the procedures outlined by Wu et al. [19] with the following exceptions. First, the thickness of the Al sheet (purity of 99%) was increased to 1 mm to avoid deformation of master molds during demolding. Second, the electro-polishing of the annealed Al sheet was performed from –5°C to 0°C for 5 min. Third, anodization was performed at 185 V in a 4:1 v/v solution of 1 wt.% phosphoric acid ($H_3PO_4$) and ethanol ($C_2H_5OH$) vigorously stirred at 600 rpm. Fourth, the solution temperature ranged from –10°C to 10°C, and ethanol was used because of its cooling effect [20]. Finally, wet etching was performed in 6 wt.% $H_3PO_4$ at room temperature or slightly higher.

## 2.4 Replicate molds

Figure 3B illustrates the fabrication process flow of the replicate molds. Master molds were pretreated using a release agent (OPTOOL HD 2100, Daikin Co. Ltd., Osaka, Japan) prior to molding. A hard PDMS (X-32-3095, Shin-Etsu Chemical Co. Ltd. Tokyo, Japan) was preferred for molding. The quantity of PDMS should be controlled, allowing the replicate molds to have a suitable thickness for better

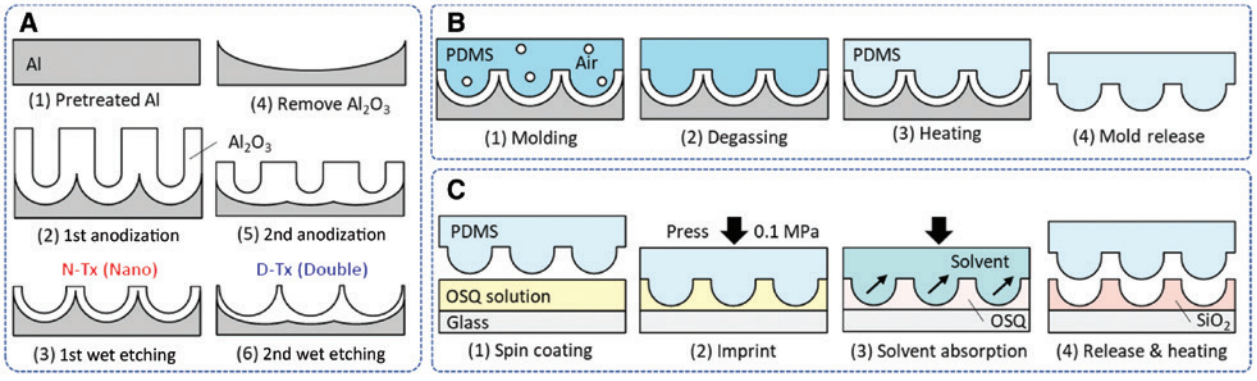


**Figure 3:** Schematic illustration of fabrication process: (A) master molds, (B) replicate molds, (C) textured substrates.

performance of the nanoimprint. After degassing, PDMS was hardened by heating at 150°C for 30 min. The dimension of the replicate mold might be slightly smaller than the glass substrate, which helps mold position when imprinting. In this study, the imprint area is slightly less than 20 mm × 20 mm to fit the size of a counter electrode.

### 2.5 Textured glass substrates

Figure 3C shows the fabrication process of textured glass substrates. The OSQ solution (Tokyo Ohka Kogyo Co. Ltd. Tokyo, Japan) was spin coated on glass substrate (Eagle XG, Corning Inc., New York, NY, USA). The spin-coating condition depends on temperature and humidity because the organic solvent of OSQ solution volatilizes rapidly. Further, a stable experimental environment is strongly recommended. A PDMS replicate mold was pressed on the OSQ solution at a pressure of 0.1 MPa at room temperature. As the solvent was absorbed by the PDMS, the texture on the replicate mold formed on the OSQ layer. Finally, after releasing the mold, the glass substrate with OSQ layer was heated at 150°C for 60 min, 250°C for 30 min, and 480°C for 30 min. The OSQ exhibited a similar characteristic to that of $SiO_2$ as a result of heat treatment.

### 2.6 Application for DSSCs

Textured substrates with a dimension of 20 mm × 20 mm × 0.7 mm were utilized for DSSC fabrication. First, the FTO film with a thickness of 700–800 nm was deposited on textured substrates using SPD, which was performed in the SPD Laboratory Inc., Hamamatsu, Japan. Moreover, $TiO_2$ deposition was performed by screen printing using a paste (Ti-Nanoxide T/SP, Solaronix, Aubonne, Switzerland) containing nanoparticles with a diameter of 15–20 nm. The thickness of the $TiO_2$ layer was approximately 4.3 μm after heating at 120°C for 30 min and 480°C for 30 min. A flat $TiO_2$ ($TiO_2$ electrode without texture) was also fabricated for comparison. Second, the substrates were immersed in N749 dye (triisothiocyanato-(2,2′:6′,6″-terpyridyl-4,4′,4″-tricarboxylato) ruthenium(II) tris(tetra-butylammonium), Solaronix) for 24 h and then rinsed with ethanol. Third, the $TiO_2$ electrodes were manually sealed with counter platinum electrodes (Solaronix, made from TCO22-7 FTO-coated glass) using a hot-melt film (Meltonix 1170-60, Solaronix) at 110°C under pressure. Finally, after electrolyte (Iodolyte HI-30, Solaronix) filling and sealing of holes, the DSSCs with an active area of 0.36 $cm^2$ (0.6 cm × 0.6 cm) were achieved.

## 3 Results and discussion

### 3.1 Textured glass substrates

To confirm the completion of the nanoimprint, the surface topography of the AAO master molds and $SiO_2$ textures were observed using a scanning electron microscope (SEM, Miniscope® TM3030, Hitachi High-Technologies Corp., Tokyo, Japan). To evaluate the AR effect and haze of textures, the reflectance and transmittance of the glass substrates with and without textures were measured using a UV/vis spectrophotometer with an integrating sphere system (V-570, JASCO, Hatchioji, Japan). In addition, to verify the improvement of the $TiO_2$ surface area at the FTO/$TiO_2$ interface, the SEM images of the FTO substrates were provided, as shown in Figure 4. To estimate

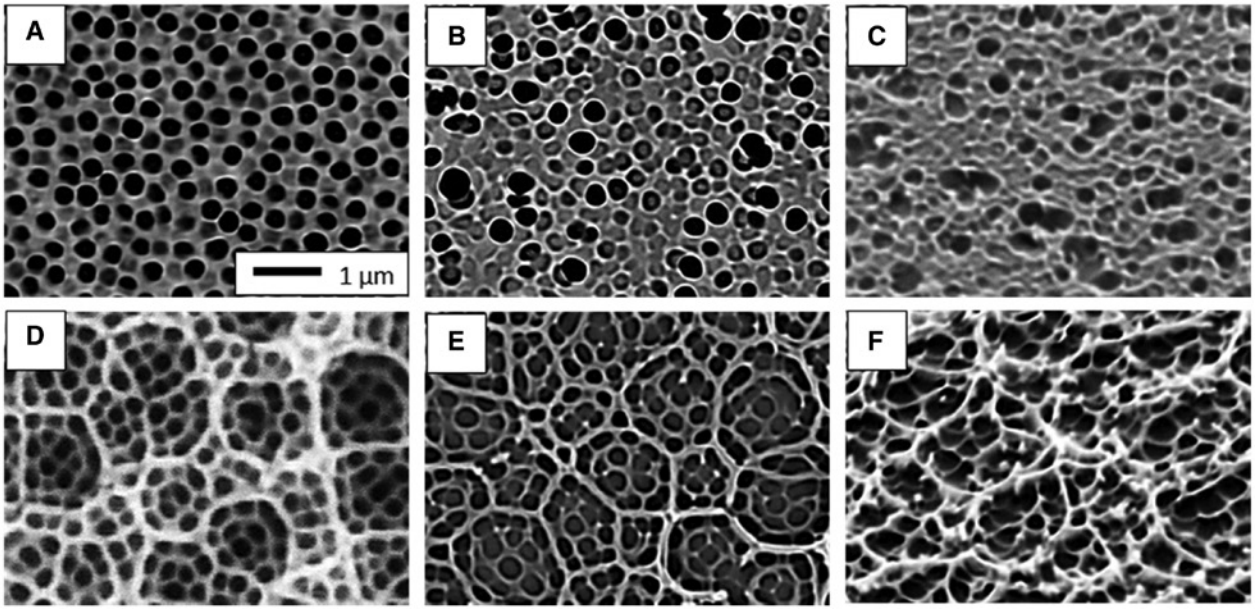


**Figure 4:** SEM images of AAO templates and SiO textures: (A) top view of N-Tx AAO; (B, C) top view and bird's eye view of N-Tx SiO; (D) top view of D-Tx AAO; (E, F) top view and bird's eye view of D-Tx SiO.

light scattering within the $TiO_2$ layer, the diffuse transmittance of the FTO substrates was analyzed. Finally, the reflectance of the $TiO_2$ substrates was evaluated to confirm the total AR effect.

Figure 4 presents the SEM images of the surface topography of the AAO master molds and $SiO_2$ textures fabricated using nanoimprint (Figure 4). Figure 4A and B illustrates that the pitch and diameter of N-Tx is approximately 200–400 nm, although not strictly periodical. The three-dimensional structure of N-Tx was verified by a bird's view image shown in Figure 4C. Uniform depth is difficult to achieve due to the features of anodization and wet etching. Figure 4D–F illustrates the hierarchical morphology of D-Tx. The nano-scale textures formed in the micro-scale templates, resembling several nets tangled together. In summary, both N-Tx and D-Tx were well replicated from the master molds to the $SiO_2$ layer on glass substrates.

The optical curves of textured glass substrates and average values in a visible wavelength with a range of 400–800 nm are shown in Figure 5. In the figure, the inner AR effect of the $SiO_2$ textures was verified by a 2.1% reflectance reduction of N-Tx and a 1.5% decrease of D-Tx. Note that the $SiO_2$ textures were fabricated between glass and air, resulting in a gradual refractive index change at the glass/air interface. The refractive index of $SiO_2$ is 1.41, which is in between the glass and air. The texture structure also provides a mild transition. In addition, the textures demonstrated high haze, indicating a long light path length caused by scattering. Generally, for either N-Tx or D-Tx, the inner AR effect is significant in a long-wavelength range (600–800 nm), and high haze appears in a short-wavelength range. Therefore, for DSSC fabrication, we chose the N749 dye that has absorption peaks over a broad range.

## 3.2 Textured FTO and $TiO_2$ substrates

Figure 6 presents the top view SEM images of FTO substrates (Figure 6). As observed in the figure, textured FTO substrates contain a rough topography than the FTO substrates without texture, although the original N-Tx and D-Tx did not appear on the FTO surface completely. Those were caused by the wettability effect of the FTO precursor on the textures' structure. We could claim that the surface area of the FTO substrates was improved with textures, indicating that the $TiO_2$ layer will have a large contact area with the FTO layer. Hence, the $TiO_2$ surface area will increase.

Figure 7 shows the optical measurement results of textured FTO and $TiO_2$ substrates. For either N-Tx or D-Tx, the total transmittance of textured FTO substrate was lower than the flat FTO (FTO substrates without texture) (Figure 7). However, a significant improvement

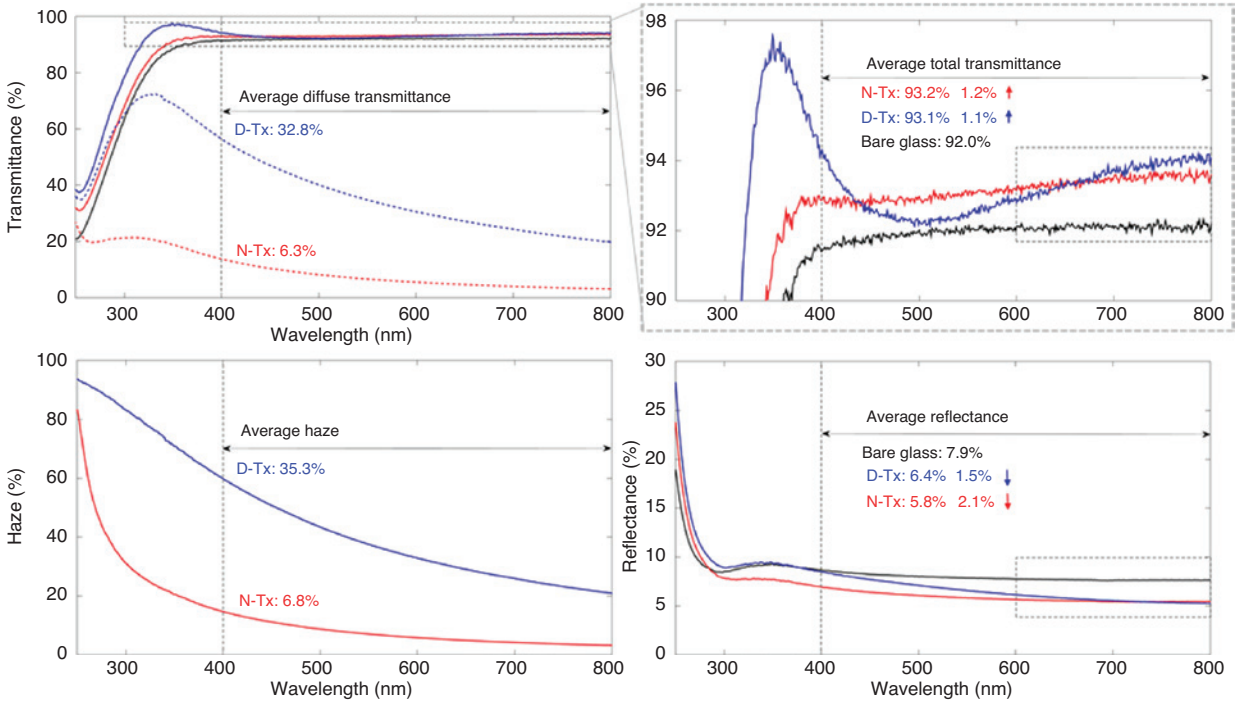


**Figure 5:** Optical measurement results of textured glass substrates.

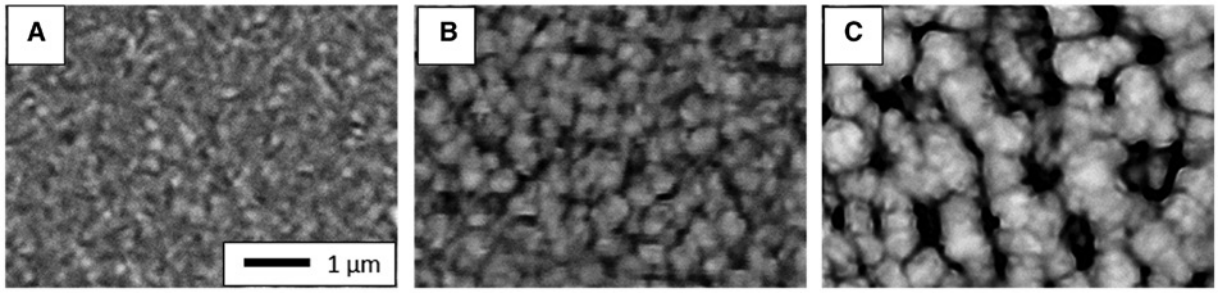


**Figure 6:** Top view SEM images of FTO substrates: (A) flat FTO (without texture); (B) with N-Tx; (C) with D-Tx.

in haze indicates that light utilization rate within the $TiO_2$ layer will increase despite the reduction in quantity. Furthermore, the average reflectance of textured $TiO_2$ substrates decreased by 0.1% (N-Tx) and 0.9% (D-Tx). Thus, the reflectance cutback verified the expected inner AR effect.

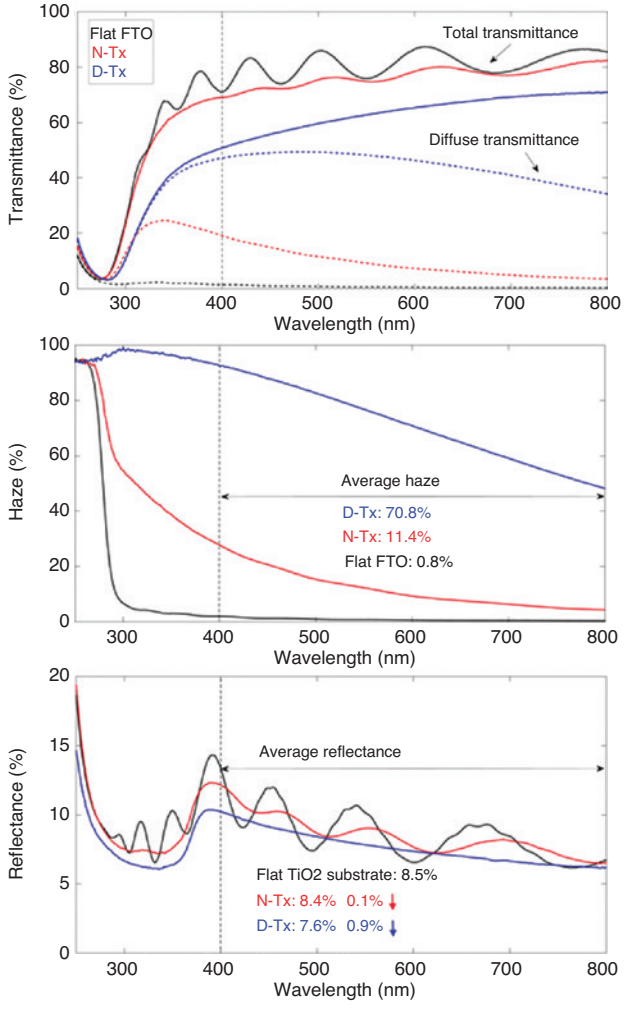


**Figure 7:** Optical measurement results of textured FTO substrates and $TiO_2$ substrates.

## 3.3 DSSCs with textured glass

Figure 8 and Table 3 illustrate the characteristics of DSSCs (Figure 8 and Table 3). The I-V curves measurement of the DSSCs was performed under STC conditions (AM 1.5, 1 SUN, 25°C) using a solar simulator (XES-155 S1, Sanei Denki Co., Ltd., Osaka, Japan). As observed in the table and figure, the short circuit current density ($J_{sc}$) in all the DSSCs fabricated in this research is lower than conventional DSSCs because $TiO_2$ is thin (4.3 μm). Moreover, the $J_{sc}$ of N-Tx and D-Tx is larger than that of flat FTO. Meanwhile, the open circuit voltage ($V_{oc}$) did not change. Besides, the fill factor (FF) of these DSSCs also did not change. Thus, the conversion efficiency of textured DSSCs improved by 11.4% (N-Tx) and 10.0% (D-Tx), compared with the flat DSSC (DSSCs without texture). The performance of DSSCs was enhanced owing to texture application, resulting in the

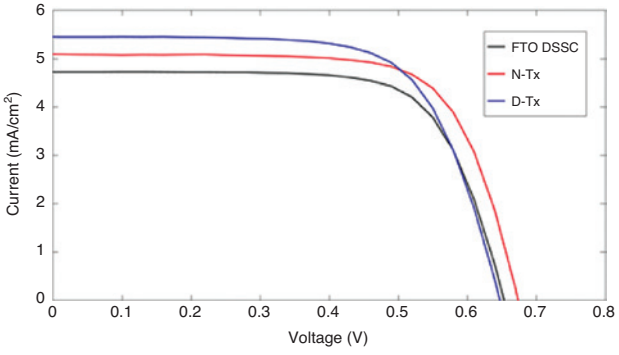


**Figure 8:** Current density–voltage curve of DSSCs.

**Table 3:** Characteristics of DSSCs.

| DSSC type | Flat | N-Tx | D-Tx |
|---|---|---|---|
| η (%) | 2.19 | 2.44 | 2.41 |
| $J_{sc}$ (mA/cm²) | 4.73 | 5.10 | 5.45 |
| $V_{oc\,(V)}$ | 0.65 | 0.67 | 0.65 |
| FF | 0.71 | 0.71 | 0.68 |

improvement of light path length and $TiO_2$ surface area. Moreover, the proposed textured substrate may be suitable for DSSC, as FF was not decreased by textured glass. The FF of other thin-film solar cells was decreased largely by texture glass [8, 9].

## 4 Conclusions

In this research, we fabricated $SiO_2$ textures on a front glass/FTO interface for DSSCs. Textured DSSCs achieved 11.4% (N-Tx, nano-texture) and 10% (D-Tx, double texture) improvement in conversion efficiency. This attempt indicated the potential of enhancing the DSSC efficiency by adding textures on the front glass/FTO interface. The reflectance of $TiO_2$ electrodes decreased due to the inner AR effect of the textures. The effect is not significant but at least not harmful when compared with traditional outer AR. The $SiO_2$ textures caused light scattering, resulting in light loss in the FTO layer. However, textures also appeared at the FTO/$TiO_2$ interface, not completely but sufficient to render the FTO surface rough. The rough FTO surface provides high haze to improve the light path length and large $TiO_2$ surface area. Consequently, the DSSCs with textured $TiO_2$ electrodes obtained better performance.

Texture fabrication was realized through PDMS NIL. Both simple N-Tx and complicated D-Tx were successfully replicated, although the characteristic in vertical direction is difficult to evaluate because of the thin thickness and random feature of the textures. Master molds were generated from the AAO templates. By adjusting the time and temperature of anodization and wet etching, considerably effective condition and different textures can be achieved.

In any case, this work was conducted roughly to confirm the possibility of inner AR textures. However, we believe that a highly significant result is achievable when further works are conducted.

**Acknowledgment:** This research was supported by Takahashi Industrial and Economic Research Foundation.

## References

[1] J. Lin, H. Yoshida, T. Iwahashi, T. Harada, J. Sakurai, et al., EU-PVSEC 2013, 2152–2154 (2013).
[2] J. Lin, J. Cashmore, T. Iwahashi, J. Sakurai, P. Losio, et al., Abstract of the 40th IEEE-Photovoltaic Specialists Conference (IEEE-PVSC 40), #580 (2014, Denver, USA).
[3] J. H. Lim, Y. H. Ko, J. W. Leem and J. S. Yu, Opt. Exp. 23, A169 (2015).
[4] S. Y. Heo, J. K. Koh, G. Kang, S. H. Ahn, W. S. Chi, et al., Adv. Energy Mater. 4, 1300632 (2014).
[5] M. Rubin, Sol. Energy Mater. 12, 275–288 (1985).
[6] C. Haase and H. Stiebig, Appl. Phys. Lett. 91, 061116 (2007).
[7] R. Dewan, M. Marinkovic, R. Noriega, S. Phadke, A. Salleo, et al., Opt. Exp. 17, 23058–23065 (2009).
[8] J. B. Orhan, R. Monnard, E. V. Sauvain, L. Frsquet, D. Romang, et al., Sol. Energy Mater. Solar Cells 140, 344–350 (2015).
[9] C. Battaglia, J. Escarre, K. Söderström, L. Emi, L. Ding, et al., Nano Lett. 11, 661–665 (2011).
[10] J. Meier, S. Dubail, S. Golay, U. Kroll, S. Faÿ, et al., Sol. Energ. Mater. Sol. C 74, 457–467 (2002).
[11] S. I. Noh, H. J. Ahn and D. H. Riu, Ceramics Int. 38, 3735–3739 (2012).
[12] Q. H. Li, D. Zhu, W. Liu, Y. Liu and X. C. Ma, Appl. Sur. Aci. 254, 2922–2926 (2008).
[13] T. Iwahashi, M. Morishima, T. Fujibayashi, R. Yang, J. Lin, et al., J. Appl. Phys. 118, 145302 (2015).
[14] M. A. Green, Y. Hishikawa, E. D. Dunlop, D. H. Levi, J. Hohl-Ebinger, et al., Prog. Photovolt. Res. Appl. 27, 3–8 (2019).
[15] F. Wang, N. K. Subbaiyan, Q. Wang, C. Rochford, G. Xu, et al., Appl. Mater. Interfaces 4, 1565–1572 (2012).
[16] W. Jiang, H. Liu, L. Yin, Y. Shi and B. Chen, J. Phys. Chem. C 120, 9678–9684 (2016).
[17] A. Knott, X. Liu, O. Makarovskiy, J. O'sea, C. Tuck, et al., Build Simul. 12, 41–49 (2019).
[18] M. J. Yun, Y. H. Sim, S. I. Cha, S. H. Seo and D. Y. Lee, Sci. Rep. 7, 15027 (2017).
[19] S. Foster and S. John, Energy Environ. Sci. 6, 2972–2983 (2013).
[20] S. Li, J. Xu, W. Wang, I. Mathews, D. O'Mahony, et al., IEEE Trans. Nanotech. 13, 537–540 (2014).
[21] Y. Igaku, S. Matsui, H. Ishigaki, J. Fujita, M. Ishida, et al., Jpn. J. Appl. Phys. 41, 4198–4202 (2002).
[22] S. J. Wilson and M. C. Hutley, Opt. Acta 29, 993–1009 (1982).
[23] A. Gombert, W. Glaubitt, K. Rose, J. Dreibholz, B. Bläsi, et al., Thin Solid Films 351, 73–78 (1999).
[24] A. P. Li, F. Müller, A. Birner, K. Nielsch and U. Gösele, J. Appl. Phys. 84, 6023–6026 (1998).
[25] J.-T. Wu, W.-Y. Chang and S.-Y. Yang, J. Micromech. Microeng. 20, 075023 (2010).
[26] Y. Li, M. Zheng, L. Ma and W. Shen, Nanotechnology 17, 5101–5105 (2006).